Regioselectivity of non-Symmetrical Borylated Dienes via EnT Catalysis: Unveiling the Relationship between Structure and Reactivity

Hao Fang[ab], Alejandro García-Eguizábal[c], Constantin G. Daniliuc[d], Ignacio Funes-Ardoiz[c]* and John J. Molloy[a]*

[a]Department of Biomolecular Systems, Max-Planck-Institute of Colloids and Interfaces, 14476 Potsdam, Germany
[b]Department of Chemistry and Biochemistry, Freie Universität Berlin, 14195 Berlin, Germany
[c]Department of Chemistry, Instituto de Investigación Química de la Universidad de La Rioja (IQUR), Universidad de La Rioja Madre de Dios 53, 26004 Logroño, Spain
[d]Organisch-Chemisches Institut, Universität Münster, 48419 Münster, Germany

Abstract: Energy transfer catalysis (EnT) has had a profound impact on contemporary organic synthesis enabling the construction of higher in energy, complex molecules, via efficient access to the triplet excited state. Despite this, intermolecular reactivity, and the unique possibility to access several reaction pathways via a central triplet diradical has rendered control over reaction outcomes, an intractable challenge. Extended chromophores such as non-symmetrical dienes have the potential to undergo 2+2 cycloaddition, 4+2 cycloaddition or geometric isomerization, which, in combination with other mechanistic considerations (site- and regioselectivity), results in chemical reactions that are challenging to regulate. Leveraging spin density as a predictive tool, in combination with the use of a core functionality that can be adequately tuned to potentially modulate reactivity, would be highly enabling in revealing the intimate links between core structure and EnT induced reactivity. Herein, we utilize boron as a tool to explore reactivity of non-symmetrical dienes under EnT catalysis, paying particular attention to the impact of boron hybridization effects on the target reactivity. Through this, a highly site- and regioselective 2+2 cycloaddition was realized with the employed boron motif effecting reaction efficiency. Reaction divergence to enable 4+2 cycloaddition was achieved, while a counterintuitive regiodivergence was observed in geometric isomerization versus 2+2 cycloaddition. The observed reactivity was validated via an in-depth mechanistic investigation determining the origin of reactivity and regiodivergence in competing EnT processes and revealing the intimate links between structure and reactivity.

INTRODUCTION

The inception of excited-state reactivity paradigms that overcome thermodynamic constraints in the ground-state have been instrumental in advancing contemporary organic synthesis. Here, light can be harnessed to facilitate the efficient photochemical or photocatalytic activation of low energy abundant feedstock chemicals to construct higher in energy, strained complex chemical systems.[1] In this regard, the light induced 2+2 cycloaddition of alkenes to form cyclobutanes, is perhaps most renown (Figure 1A),[2] enabling the facile translation from 2D to 3D chemical space,[3] constructing up to four contiguous stereocentres in a single process. Despite these advances, many intractable challenges that plague intermolecular reactivity, persist, often leading to uncontrolled reactivity/selectivity (Figure 1A, bottom). These challenges include, competing homodimerization due to self 2+2 cycloaddition,[4] formation of regioisomers as a result of differences in alkene approach, and variation in diastereoselectivity attributable to formed radical intermediates.[2,5] Pioneering research has made notable strides in addressing such limitations enabling catalysis via non-covalent interactions[6] or substrate control.[7] Lewis acids or Brønsted acids have been leveraged, leading to concomitant enantioinduction,[8] while advances in photocatalyst design has seen the inception of quantum dots,[9] and chiral frameworks,[10] to provide a wide platform of compatible precursors that are operational.

The translation to non-symmetrical dienes poses additional aspects that hinder reaction selectivity (Figure 1B, top). Upon excitation, site-selectivity of a specific alkene is a consideration, while competing reactivity can lead to reaction divergence, such as, uncontrolled “alkene scrambling”, via geometric isomerization,[11] and 4+2 cycloaddition via reactivity at both termini of the diene.[12] The result is a complex distribution of products that is challenging to modulate both photochemically or via EnT.[13] To regulate selectivity, the design of non-covalent interactions is ambitious as reaction pathways are intimately linked to intrinsic reactivity and excited

state properties of the system. When considering triplet excited states spin density is often leveraged as a predictive tool for regioselectivity with great effect,[14] however, application with non-symmetrical dienes is comparatively underexplored. The strategic incorporation of a single unit that can be systematically tuned to display contrasting reactivity would be highly enabling to probe spin density and competing reaction pathways, providing a user's guide for future reaction design of non-symmetrical diene systems.

Organoboron species can readily exist in two discrete hybridized forms that exhibit stark differences in excited state reactivity (Figure 1C, top).[15] In its trigonal planar form boron has been shown to enable efficient EnT,[16] due to conjugation of the boron p-orbital, while occupation via a dative interaction forming the tetrahedral boronate has rendered boron less efficient to sensitization.[15a] In addition, hybridization has been shown to influence the intrinsic reactivity of α-boryl radicals,[16] and consequently, we envisaged this would be an ideal model system to probe reaction pathways of non-symmetrical dienes. Specifically, we looked to explore if the boron motif, or hybridization state, has the potential to influence spin density upon excitation to promote alternative pathways (Figure 1C, bottom), and assess what impact hybridization can have on intrinsic reactivity of the generated biradical.

Herein we describe the EnT mediated 2+2 cycloaddition of conjugated organoboron systems proceeding with excellent site-selectivity, regioselectivity and diastereoselectivity (Figure 1D). The judicious choice of a low energy catalyst system mitigates "alkene scrambling" to limit reaction outcomes to a single geometric isomer. Systematic analysis of boron substituents unveils a clear relationship between boron species and compatible alkene coupling partners, while subtle modifications of the core scaffold enabled a divergent pathway to form preferentially 4+2 cycloadducts. Mechanistic probes revealed a counterintuitive geometric isomerization with opposite regioselectivity to that of 2+2 cycloaddition, leading to an in-depth computational study to determine the intimate links between spin density, reactivity and the origin of reaction divergence.

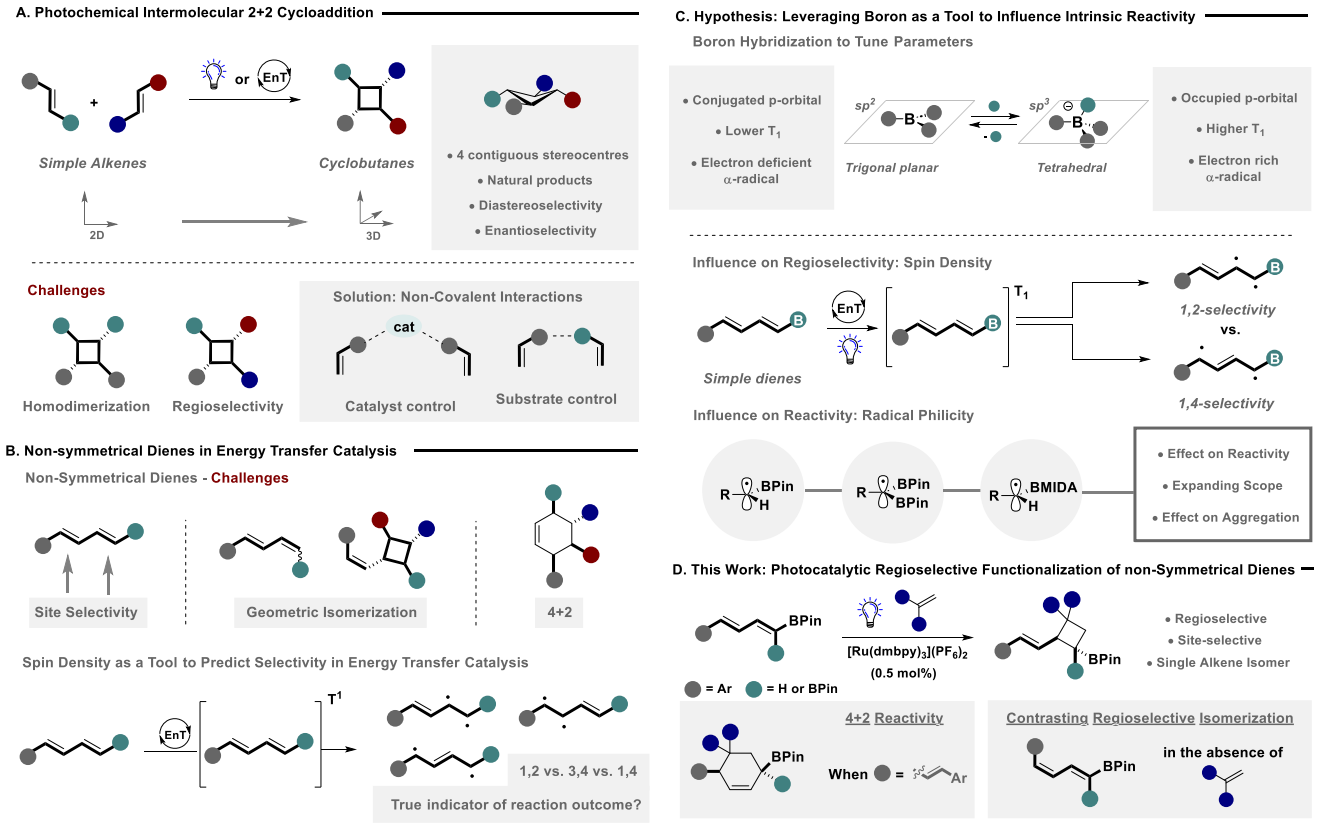

Figure 1. A) Photochemical 2+2 cycloaddition. B) Intractable challenges in photochemical 2+2 cycloaddition reactions of simple alkenes and non-symmetrical dienes. C) Exploring boron hybridization as a tool to influence the intrinsic reactivity of 2+2 cycloadditions. D) Energy transfer catalyzed 2+2 cycloaddition of non-symmetrical borylated dienes.

RESULTS AND DISCUSSION

We initiated our optimization probing the efficiency of diene **1** to undergo 2+2 cycloaddition with styrene **2** in the presence of a photocatalyst (Table 1). Utilizing a lower energy sensitizer $[Ru(dmbpy)_3](PF_6)_2$,[18] afforded 2+2 adduct ***E*-3** in appreciable yield and good regio- and site-selectivity (Entry 1). However, significant amounts of dimer **4** were generated, hindering the targeted reactivity. Implementing sensitizers of higher energy was detrimental, resulting in formation of geometrical alkene isomer ***Z*-3** (Entries 2 to 4), while also compromising diastereoselectivity (See ESI for full details). Varying styrene equivalents had little effect in suppressing dimer formation (Entries 5 and 6). Inspired by recent studies exploiting slow addition to mitigate homodimerization,[8e] we next employed a syringe pump to carefully control the concentration of diene 1 (Entry 7). Pleasingly, this regulated the formation of dimer leading to excellent yields of 2+2 heteromer. Carrying out the reaction under an air atmosphere supported a triplet EnT process (Entry 8), while control reactions demonstrated that catalysis is operational (Entries 9 and 10).

Table 1. Optimisation of reaction conditions.[a]

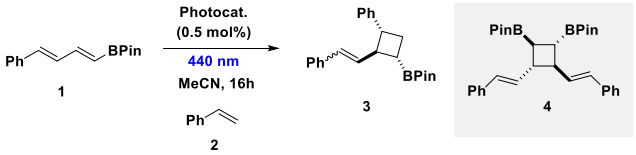

Entry	Catalyst	E_T[17] (kcal/mol)	***E*-3** (%)[b]	***Z*-3** (%)[b]	**4** (%)[b]
1	$[Ru(dmbpy)_3](PF_6)_2$	45.3	41	-	26
2	$[Ir(ppy)_2(dtbpy)]PF_6$	49.2	20	20	15
3	$Ir(ppy)_3$	55.2	10	30	-
4	$Ir(dFppy)_3$	60.1	-	-	-
5[c]	$[Ru(dmbpy)_3](PF_6)_2$	45.3	28	-	23
6[d]	$[Ru(dmbpy)_3](PF_6)_2$	45.3	58	-	19
7[e]	**$[Ru(dmbpy)_3](PF_6)_2$**	**45.3**	**95**	-	**< 5**
8[e,f]	$[Ru(dmbpy)_3](PF_6)_2$	45.3	78	-	-
9[e]	-	-	-	-	-
10[e,g]	-	-	trace	-	-

a) Standard conditions: **1** (0.1 mmol), **2** (20 equiv), cat. (0.5 mol%), MeCN (0.2 M), rt 16 h, Kessil lamp 10 W. b) Determined by ^{1}H NMR spectroscopy against a known internal standard (1, 3, 5-trimethoxybenzene). c) 5 equiv. of **2** was used. d) 50 equiv. of **2** was used. e) **1** dissolved in 0.4 mL added via syringe pump 0.001 mL/min. f) Oxygen atmosphere. g) 370 nm lamp used.

Having established conditions that promote the target reactivity we next set out to determine the scope and compatibility of the model system (Scheme 1). For all reactions assessed, site-, regio- and alkene *E*/*Z* selectivity was comprehensively in favor of one product. Our model reaction led to the generation of four diasteromers favoring an *anti* relationship between aryl and styrenyl substituents and *anti* for styrene and boron motif (**3**). Translation to 1,1-disubstituted styrenes was tolerated in good yield and diastereoselectivity (**5**), while electron-rich dienes were also compatible in the *ortho*, *meta* and *para* positions (**6** to **8**). The incorporation of heterocycles, such as furan, proceeded in good yield resulting in a slight erosion of diastereoselectivity (**9**). Inductively and mesomerically electron withdrawing motifs were also tolerated in the diene scaffold with little effect on reactivity or selectivity (**10** to **14**), while modifications of the 1,1-diphenyl ethylene coupling partner were also effective (**15**). However, to our great surprise, extending the chromophore to a triene system activated an alternative reaction pathway generating an intermolecular 4+2, skipped diene product, whose structure was conclusively determined via x-ray analysis after oxidation. It is pertinent to note at this stage,

that any deviation away from styrenyl coupling partners resulted in little to no target reactivity, favoring diene homodimerization (See ESI for full details on unsuccessful substrates).

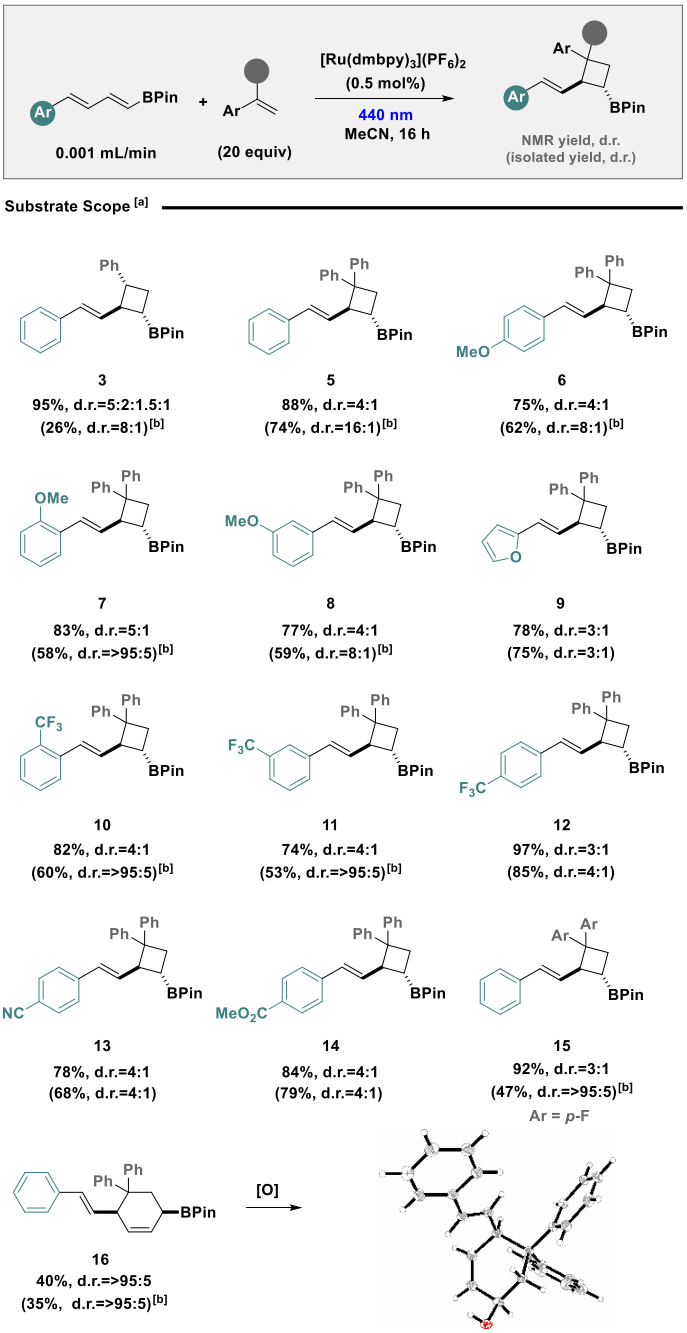

Scheme 1. Substrate scope and x-ray of compound **16**. a) Reactions were performed in MeCN on a 0.2 mmol scale using diene (1 equiv.), alkene (20 equiv.), photocat. (0.5 mol%) under 440 nm irradiation (10 W). Diene was added as a solution in MeCN via syringe pump (0.8 mL, 0.001 mL/min). NMR yield and d.r. was determined by 1H NMR spectroscopy against a known internal standard (1,3,5-trimethoxybenzene). b) To aid separation and characterization, the product was isolated after oxidation to the corresponding alcohol.

Although our developed protocol enables expedient access to synthetically useful, complex scaffolds that contain a boron and alkene handle, efficiency is contingent on the use of a syringe pump and an excess of styrene to mitigate dimerization. To gain a better understanding of the dimerization process we probed reactivity in the absence of an alkene coupling partner (Scheme 2). It was found that dimerization was rapid leading to 36% conversion (of a possible 50%) after only one hour, which we attribute to aggregation effects in solution (See ESI for full details).[19] At this stage, it was envisaged that increasing steric parameters, or modulating intrinsic reactivity of the participating double bond may be beneficial to enhance the desired

reactivity. The incorporation of an additional BPin handle, diene **17**, led to no observed homodimerization after one hour indicating its unique ability to mitigate dimerization. X-ray analysis of the geminal BPin diene **17** revealed a more sterically congested system, with one BPin motif in the plane and the other perpendicular, that likely limits aggregation (See ESI for full details).[20]

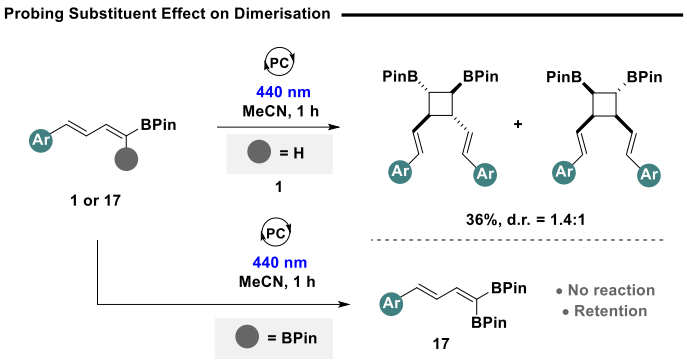

Scheme 2. Probing substituent effect on homodimerization.

Given the bespoke reactivity in homodimerization, we next assessed non-symmetrical dienes, containing a *geminal* BPin, in intermolecular 2+2 cycloadditions (Scheme 3). Subtle modifications enabled reactions to be carried out using 5 equivalents of alkene coupling partner without the necessity of a syringe pump, further underpinning the unique reactivity of the geminal system. The reaction was tolerant to modifications of the diene aromatic ring (**18** to **21**), generating the cycloadduct in good yield, while incorporation of functionality in the alkene coupling partner was also effective (**22** and **23**). The protocol was amenable to simple styrene and diene coupling partners affording the *syn* diastereomer as the dominant product (**24** to **26**). Intriguingly, in stark contrast to the mono-substituted system **1**, electron deficient Michael acceptors were efficient (**27**). Electron deficient alkenes were compatible with various dienes including electron-rich (**28**), electron-poor (**29**) and heterocycles (**30**). Moreover, varied alkenes could be employed, including bulkier acrylates (**31**), acrylonitrile (**32**) and methyl methacrylate (**33**). The use of a borylated alkene enabled the synthesis of polyboronate structure (**34**).[15g] The scope culminated in the synthesis of bicyclopentane **35**,[21] granting expedient access to a 3D framework containing a Weinreb amide, an alkene, and a *geminal* boronic ester for further downstream synthetic manipulations.

The boron p-orbital has been shown to serve a prominent role in regulating EnT catalysis.[15] As such, we anticipated that moving to a tetrahedral boronate hybridization state may have an adverse effect on excited state energy, resulting in reaction inhibition. However, to our surprise, the use of a BMIDA moiety **36** had little to no effect on reactivity (Scheme 4A),[22] forming the target cyclobutane **37** with enhanced diastereoselectivity in comparison to the analogous boronic ester **1**. This probe indicates that excitation efficiency is contingent solely on conjugation of the diene system and is not regulated by the boron p-orbital. Indeed, the reaction was shown to be comprehensively selective with alternative functionalities (Scheme 4B), including electron withdrawing groups (**38** and **39**) or in the absence of any substituent (**40**). While further reaction probes of substrate **36** confirmed inefficient homodimerization (Scheme 4b), this also unveiled an unexpected geometric isomerization process that counterintuitively occurred at the alternative alkene site to that of which 2+2 cycloaddition occurs (Scheme 4b). This result was particularly intriguing, given that comprehensive selectivity of the *E*-isomer product is obtained after 2+2 cycloaddition (Scheme 4a). The observed anomaly inspired us to embark on an in-depth mechanistic analysis to reveal the origin of site selectivity and reaction divergence.

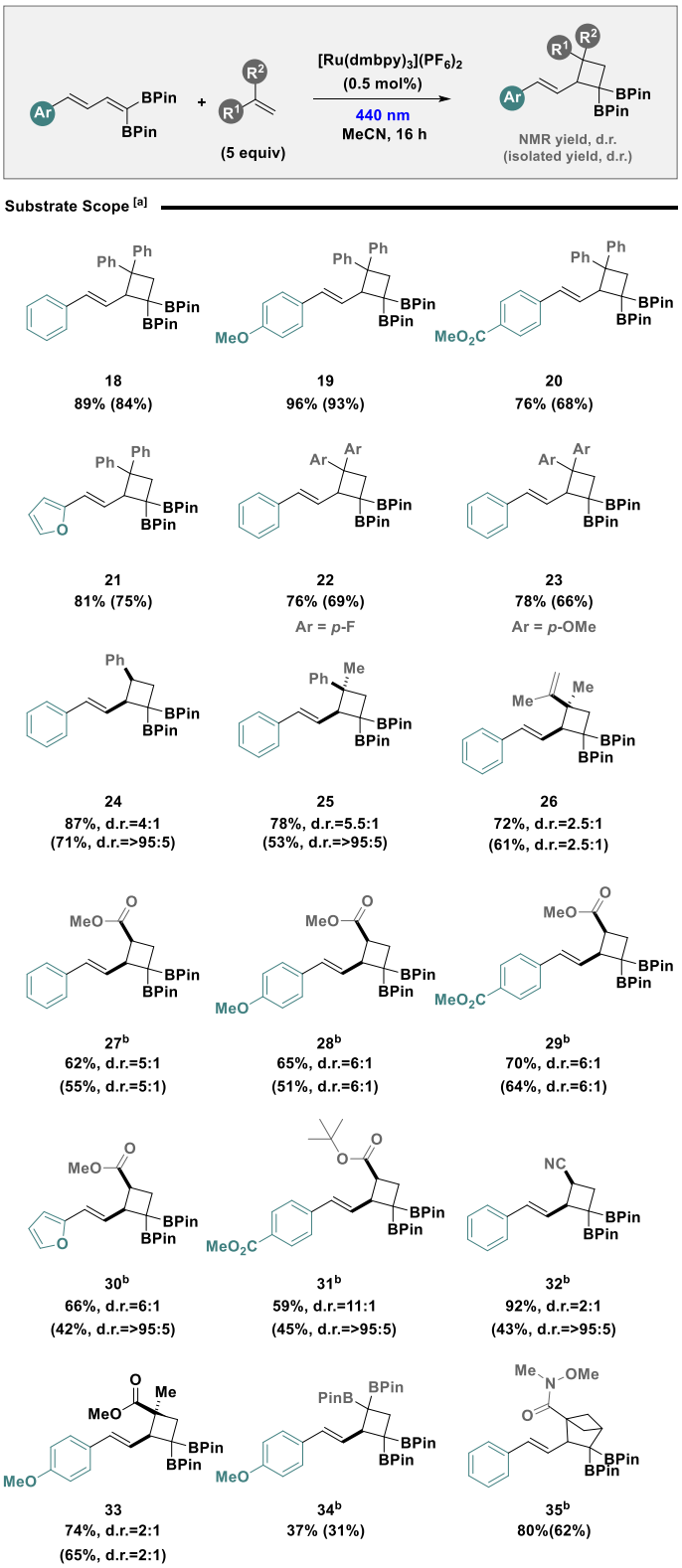

Scheme 3. Establishing substrate scope. a) Reactions were performed in MeCN on a 0.2 mmol scale using diene (1 equiv.), alkene (5 equiv.), photocat. (0.5 mol%) under 440 nm irradiation (10 W). NMR yield and d.r. was determined by 1H NMR spectroscopy against a known internal standard (1,3,5-trimethoxybenzene). b) 10 equiv. of alkene was used.

To assess the generality of the geometric isomerization and to ensure the observed regioselectivity was not unique to BMIDA system **36**, alternative dienes were first probed under model reaction conditions (Figure 2A). Exposing diene **1** to the photocatalyst and light irradiation for one minute resulted in a rapid isomerization, with identical regioselectivity to that of BMIDA substrate **36**. The strategic incorporation of an α-methyl (41)

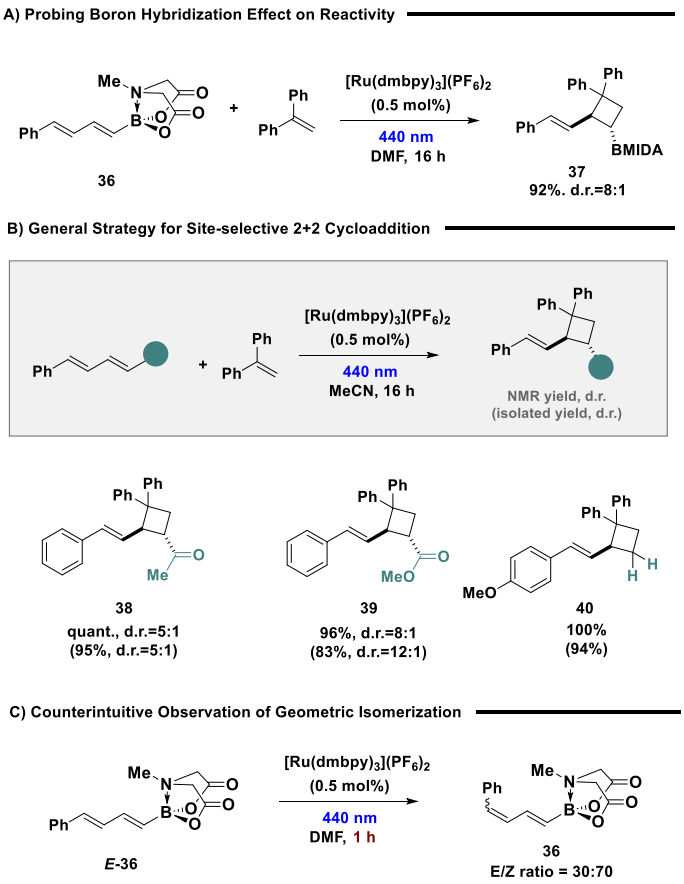

Scheme 4. Probing the importance of the boron p-orbital.

and *ortho* substitutent (**42**), known to enhance isomerizazion via a buildup of 1,3-allylic strain,[23] also led to comparable alkene isomerization. These results instilled confidence that regiodivergence of the two EnT processes is general. To gain a deeper insight into the reaction profile we next carried out reaction monitoring (Figure 2B), quantifying the presence of starting material **(*E*),(*E*)-41** (red), isomerization product **(*Z*),(*E*)-41** (grey), and 2+2 cycloaddition product **43** (green). Analyzing the initial 15 minutes of the reaction revealed a rapid alkene isomerization process showing the clean conversion of **(*E*),(*E*)-41** to **(*Z*),(*E*)-41** with minimal 2+2 cycloaddition observed (Figure 2B, i). However, running the reaction for an extended period demonstrated the depletion of **(*Z*),(*E*)-41** and formation of cycloadduct **43** (Scheme 2B, ii). It is pertinent to note that during reaction monitoring, no other geometric isomers of diene starting material or product were detected and substrates with higher *Z*:*E* ratios were slower to undergo 2+2 cycloaddition, which aligns with recent advances in 2+2 reactions of imine derivatives.[24] As a control **(*Z*),(*E*)-41** was synthesized independently and exposed to the model reaction conditions (Figure 2C). Again, clean translation from (*Z*),(*E*)-starting material to geometrically pure *E*-isomer product was observed. Further controls were carried out demonstrating that the employed ruthenium catalyst does not facilitate a *Z*→*E* isomerization of the product styrene scaffold (See ESI for full details). Cyclic voltammetry ruled out possible single electron transfer providing further evidence of a sensitization activation mode (See ESI for full details). While, these seminal reaction probes unveil the systematic order in which reactivity occurs, rapid isomerization and slower subsequent 2+2 cycloaddition, they provide very little in distilling the origin of regiodivergence.

To further assess the observed reactivity, a computational investigation of the reaction was initiated. We focused on examining the mechanism of the different 2+2 cycloadditions through DFT calculations paying particular attention to the excellent site-selectivity, regioselectivity and diastereoselectivity. For this purpose, the mechanistic pathway of cycloadduct **5** formation was explored at the SMD (MeCN) ωB97xD/Def2TZVPP//ωB97xD/Def2SVP level of theory in Figure 3 (full computational details can be found in the Supporting Information). Upon sensitization of substrate, the generated triplet diradical state can undergo

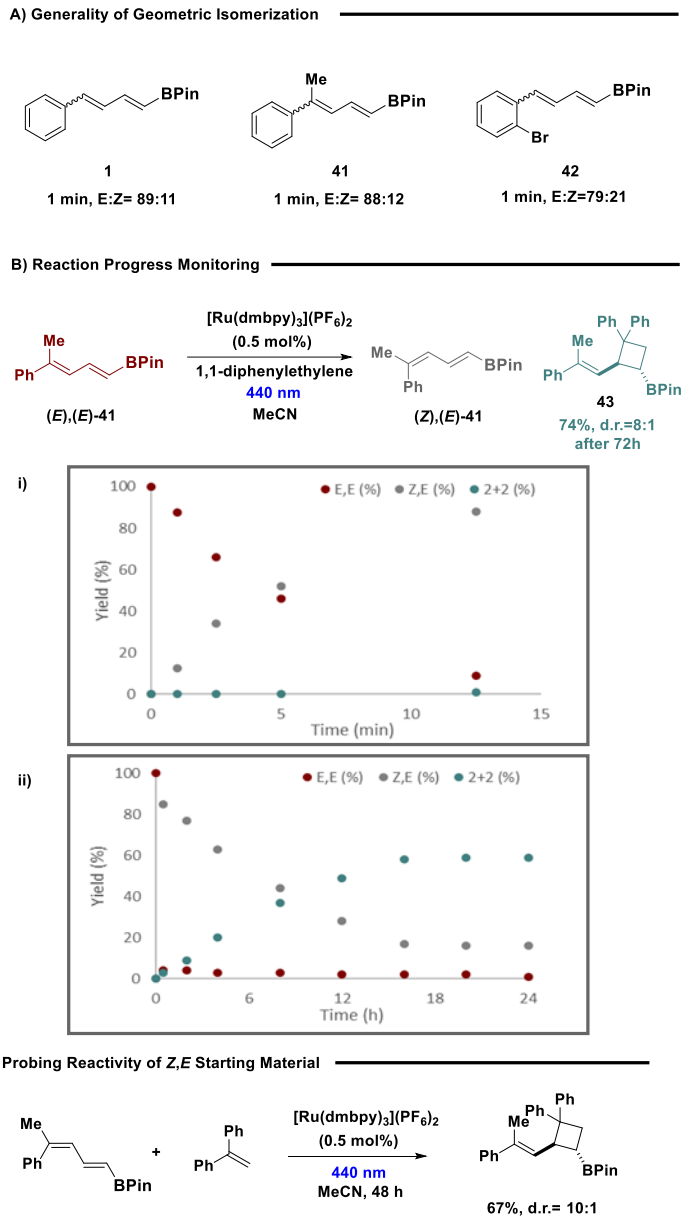

Figure 2. Mechanistic investigation of observed reaction divergence.

a site-selective bond rotation to generate the more stable $^{3}\mathbf{1}_{Z}$ structure through a minimal free energy barrier of 1.4 kcal/mol.[25] Excited diradical $^{3}\mathbf{1}_{Z}$ can then return to the ground state to form the corresponding (*Z*),(*E*)-isomer via radical recombination. Reexcitation of (*Z*),(*E*)-isomer with varying efficiency generates a dynamic photostationary state equilibrium between both geometrical isomers which is substrate dependent. This is in agreement with the rapid, site selective geometric isomerization observed experimentally for the different alkenes explored in Figure 2. In the triplet excited state, spin density is primarily located at both termini of the diene; at the carbon adjacent to boron and delocalized between the aromatic ring and the benzylic position. While this supports specifically neither isomerization nor 2+2 cycloaddition, rendering spin density as an inaccurate tool for regioselectivity prediction, it provides an excellent basis for the subsequent step-wise reactivity that occurs. The more reactive α-boryl radical for both *Z* and *E* states can undergo a radical addition to the double bond of 1,1-diphenylethylene. Interestingly, the addition of the *E* isomer is much faster than the *Z* isomer ($\Delta\Delta G^{\ddagger}$ = 4.4 kcal/mol) and the reaction is very exergonic forming preferentially $^{3}\mathbf{2}_{\text{E-anti}}$, and making this step irreversible, defining the selectivity of the final *E* product in a Curtin-Hammet scenario, where the less stable isomer reacts faster than the most stable one. This is consistent with the fact that only one geometric isomer was observed experimentally. Two different conformers were calculated for this radical addition (see

Figure S11) and, in both cases, *endo*-like transition states were more stable than the *exo*-like ones (10.4 and 14.8 *vs* 12.8 and 15.9 kcal/mol).

From intermediate ^{3}**2**$_{E\text{-}anti}$, the ring-closing step was explored. First, the *anti* and *syn* isomers were found to be very close in energy (0.6 kcal/mol). Interestingly, the ring closing transition states in the triplet state for both isomers were prohibitively high in energy (>30 kcal/mol) due to the loss of conjugation in the diradical system, forming a 90º C-C single bond and losing the stereochemical information of the double bond, that would result in a cis-trans mixture of both *anti* and *syn* products. However, a Minimum Energy Crossing Point (MECP) was located, using the *easyMECP* software,[26] for both the *anti* and the *syn* isomers before the triplet transition states at 2.39 Å of the C-C bond formation. In both cases, once the triplet→singlet ground state transition occurs at a conical intersection, the singlet state proceeds thermodynamically downhill to products ^{1}**E-Prod**$_{anti}$ and ^{1}**E-Prod**$_{syn}$ via radical recombination. Again, the higher stability of the **MECP**$_{anti}$, due to the reduced steric hindrance, compared to the **MECP**$_{syn}$, 3.0 kcal/mol, aligns with the experimentally observed diastereoselectivity. Due to the higher excited state energy of the shorter styrene chromophore, reexcitation of the formed (*E*)-isomer via EnT is inefficient as supported by control experiments (See ESI for full details).

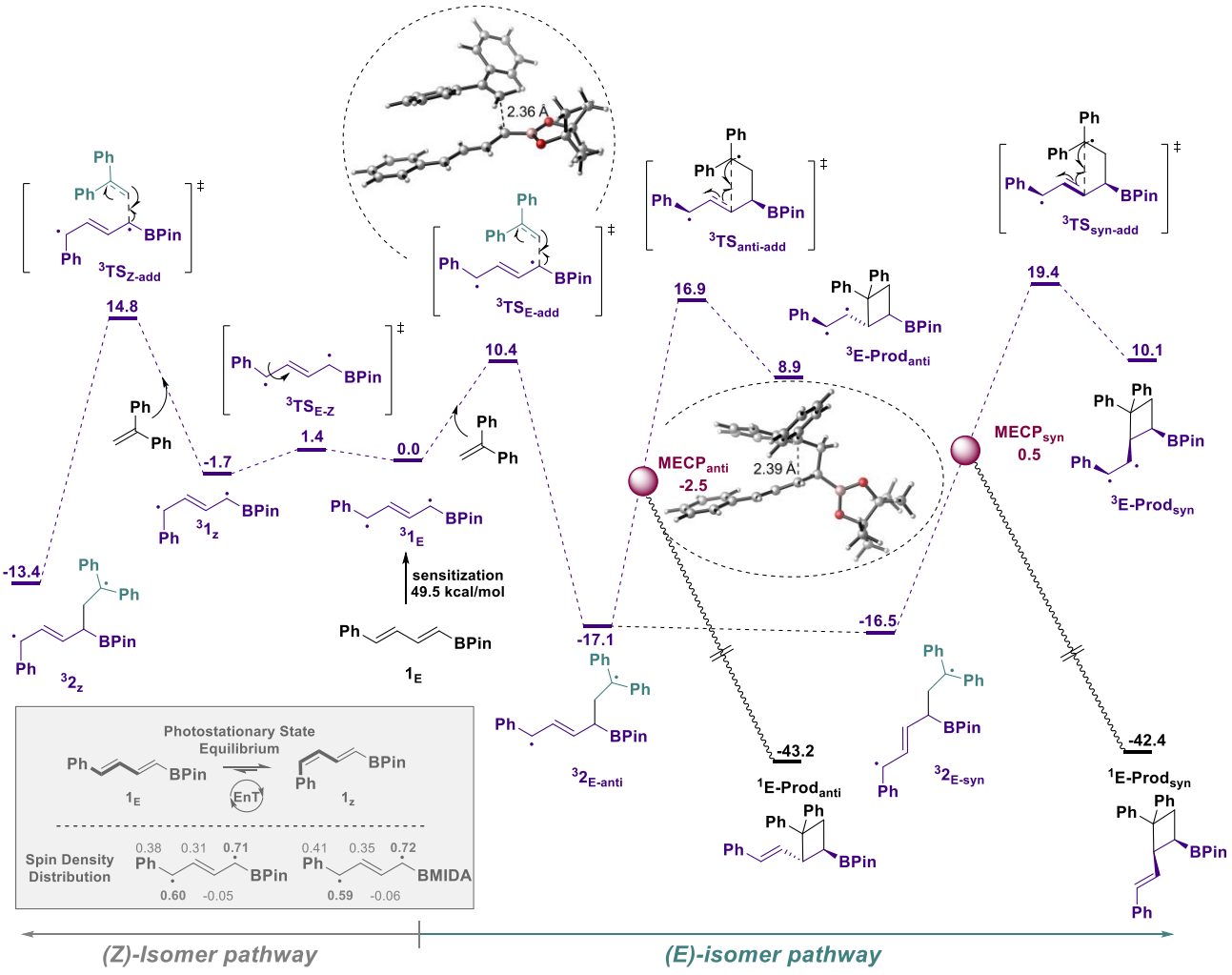

Figure 3. Free energy profile of the reaction mechanism at the ωB97xD/Def2TZVPP//ωB97xD/Def2SVP level of theory. Energies in kcal/mol and bond distances in Åmstrong.

In a bid to demonstrate the power of the developed method, *geminal* BPin products **18** and **35** were further derivatized (Scheme 5).[27] Oxidation of **18** resulted in a subsequent Bayer-Villiger reaction to afford lactone **44** in high yield, while oxidation of **35** generated bicyclic ketone **45**. Base-mediated protodeboronation,[28] furnished *syn* diastereomers **46** and **47** in high yields providing a complimentary approach to the opposite diastereomer generated under EnT catalysis (Scheme 1).

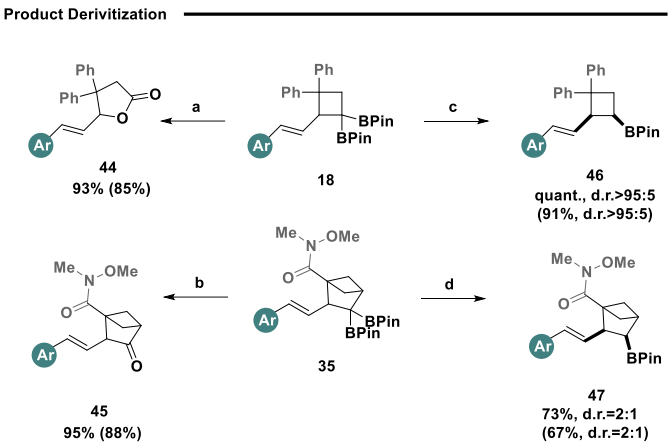

Scheme 5. Product derivatization: (a) H_2O_2, THF/H_2O, rt; (b) $NaBO_3$•H_2O (5 equiv.), THF, H_2O buffer (pH=7), 0 °C → rt; (c) KO*t*-Bu (2 equiv.), toluene, 40 °C; (d) KO*t*-Bu (2 equiv.), toluene, rt.

CONCLUSIONS

In summary, we have developed a site-, regio-, and diastereoselective 2+2 cycloaddition of non-symmetrical boron containing dienes. Systematic changes of the model system enabled 4+2 cycloaddition via extension of the chromophore, while the strategic incorporation of an additional boron unit, mitigated aggregation and enhanced reactivity. Boron hybridization proved to be ineffective, in contrast to current state of the art, in modulating EnT, yet revealed counterintuitive regiodivergence between geometric isomerization and 2+2 cycloaddition EnT processes. In-depth mechanistic analyses demonstrated a rapid site-selective geometric isomerization generating a photostationary state equilibrium between isomers, while computational investigations determined the Curtin-Hammett principle promotes preferential reactivity of the *E*-biradical with an alkene to forge specifically the target cycloadducts. Importantly, while spin density is effective in predicting electron density upon excitation, it's ability as a predictive tool, in step-wise energy transfer processes was shown to be obsolete. It is envisaged the developed insights will serve as a blueprint for the future discovery of divergent platforms utilizing non-symmetrical dienes under EnT catalysis.

Acknowledgements

We gratefully acknowledge financial support from the Max-Planck Society. J. J. M. thanks the Fonds der Chemischen Industrie, FCI for funding. J. J. M. thanks the Daimler and Benz Foundation for financial support. H. F. thanks the Chinese Scholarship Council for funding. We thank Billy Joe Buhrmeister for preliminary results and Dr. Roza Bouchal for help with cyclic voltammetry experiments. We thank Prof. Peter H. Seeberger and Andreas Schäfer for scientific discussions. We thank the Mass Spec department of Freie Universität. I. F. -A thanks the funding of PID2021-126075NB-I00 project and RYC2022-035776-I scholarship, funded by MCIN/AEI/10.13039/501100011033 and the European Union "Next Generation EU"/PRTR.

References

1. (a) Roth, H. D. The Beginnings of Organic Photochemistry. *Angew. Chem. Int. Ed.* **1989**, *28*, 1193–1207; (b) Schultz, D. M.; Yoon, T. P. Solar Synthesis: Prospects in Visible Light Photocatalysis. *Science* **2014**, *343*, 1239176; (c) Wang, H.; Tian, Y.-M.; König, B. Energy- and Atom-Efficient Chemical Synthesis with Endergonic Photocatalysis. *Nat. Rev. Chem.* **2022**, *6*, 745–755; (d) Goti, G.; Manal, K.; Sivaguru, J.; Dell'Amico, L. The Impact of UV Light on Synthetic Photochemistry and Photocatalysis. *Nat. Chem.* **2024**, *16*, 684–692.
2. Poplata, S.; Tröster, A.; Zou, Y.-Q.; Bach, T. Recent Advances in the Synthesis of Cyclobutanes by Olefin [2 + 2] Photocycloaddition Reactions. *Chem. Rev.* **2016**, *116*, 9748–9815.
3. Reymond, J.-L. The Chemical Space Project. *Acc. Chem. Res.* **2015**, *48*, 722–730.
4. Lewis, F. D.; Quillen, S. L.; Hale, P. D.; Oxman, J. D. Lewis Acid Catalysis of Photochemical Reactions. 7. Photodimerization and Cross-Cycloaddition of Cinnamic Esters. *J. Am. Chem. Soc.* **1988**, *110*, 1261–1267.

5. (a) Schuster, D. I.; Lem, G.; Kaprinidis, N. A. New Insights into an Old Mechanism: [2 + 2] Photocycloaddition of Enones to Alkenes. *Chem. Rev.* **1993**, *93*, 3–22; (b) Jung, H.; Hong, M.; Marchini, M.; Villa, M.; Steinlandt, P. S.; Huang, X.; Hemming, M.; Meggers, E.; Ceroni, P.; Park, J.; Baik, M.-H. Understanding the Mechanism of Direct Visible-Light-Activated [2 + 2] Cycloadditions Mediated by Rh and Ir Photocatalysts: Combined Computational and Spectroscopic Studies. *Chem. Sci.* **2021**, *12*, 9673–9681.
6. For recent reviews see: (a) Brimioulle, R.; Lenhart, D.; Maturi, M. M.; Bach, T. Enantioselective Catalysis of Photochemical Reactions. *Angew. Chem. Int. Ed.* **2015**, *54*, 3872–3890; (b) Xu, Y.; Conner, M. L.; Brown, M. K. Cyclobutane and Cyclobutene Synthesis: Catalytic Enantioselective [2+2] Cycloadditions. *Angew. Chem. Int. Ed.* **2015**, *54*, 11918–11928; (c) Brenninger, C.; Jolliffe, J. D.; Bach, T. Chromophore Activation of α,β-Unsaturated Carbonyl Compounds and Its Application to Enantioselective Photochemical Reactions. *Angew. Chem. Int. Ed.* **2018**, *57*, 14338–14349; (d) Großkopf, J.; Kratz, T.; Rigotti, T.; Bach, T. Enantioselective Photochemical Reactions Enabled by Triplet Energy Transfer. *Chem. Rev.* **2022**, *122*, 1626–1653; (e) Genzink, M. J.; Kidd, J. B.; Swords, W. B.; Yoon, T. P. Chiral Photocatalyst Structures in Asymmetric Photochemical Synthesis. *Chem. Rev.* **2022**, *122*, 1654–1716.
7. Liu, Y.; Ni, D.; Brown, M. K. Boronic Ester Enabled [2 + 2]-Cycloadditions by Temporary Coordination: Synthesis of Artochamin J and Piperarborenine B. *J. Am. Chem. Soc.* **2022**, *144*, 18790–18796.
8. For selected examples see: (a) Brimioulle, R.; Bach, T. Enantioselective Lewis Acid Catalysis of Intramolecular Enone [2+2] Photocycloaddition Reactions. *Science* **2013**, *342*, 840–843; (b) Poplata, S.; Bach, T. Enantioselective Intermolecular [2+2] Photocycloaddition Reaction of Cyclic Enones and Its Application in a Synthesis of (−)-Grandisol. *J. Am. Chem. Soc.* **2018**, *140*, 3228–3231; (c) Stegbauer, S.; Jandl, C.; Bach, T. Enantioselective Lewis Acid Catalyzed Ortho Photocycloaddition of Olefins to Phenanthrene-9-Carboxaldehydes. *Angew. Chem. Int. Ed.* **2018**, *57*, 14593–14596; (d) Sherbrook, E. M.; Jung, H.; Cho, D.; Baik, M.-H.; Yoon, T. P. Brønsted Acid Catalysis of Photosensitized Cycloadditions. *Chem. Sci.* **2020**, *11*, 856–861; (e) Genzink, M. J.; Rossler, M. D.; Recendiz, H.; Yoon, T. P. A General Strategy for the Synthesis of Truxinate Natural Products Enabled by Enantioselective [2+2] Photocycloadditions. *J. Am. Chem. Soc.* **2023**, *145*, 19182–19188; (f) Plachinski, E. F.; Kim, H. J.; Genzink, M. J.; Sanders, K. M.; Kelch, R. M.; Guzei, I. A.; Yoon, T. P. A General Synthetic Strategy toward the Truxillate Natural Products via Solid-State Photocycloadditions. *J. Am. Chem. Soc.* **2024**, *146*, 14948–14953.
9. (a) Jiang, Y.; Wang, C.; Rogers, C. R.; Kodaimati, M. S.; Weiss, E. A. Regio- and Diastereoselective Intermolecular [2+2] Cycloadditions Photocatalysed by Quantum Dots. *Nat. Chem.* **2019**, *11*, 1034–1040; (b) Jiang, Y.; López-Arteaga, R.; Weiss, E. A. Quantum Dots Photocatalyze Intermolecular [2 + 2] Cycloadditions of Aromatic Alkenes Adsorbed to Their Surfaces via van Der Waals Interactions. *J. Am. Chem. Soc.* **2022**, *144*, 3782–3786.
10. (a) Tröster, A.; Alonso, R.; Bauer, A.; Bach, T. Enantioselective Intermolecular [2 + 2] Photocycloaddition Reactions of 2(1H)-Quinolones Induced by Visible Light Irradiation. *J. Am. Chem. Soc.* **2016**, *138*, 7808–7811; (b) Huang, X.; Quinn, T. R.; Harms, K.; Webster, R. D.; Zhang, L.; Wiest, O.; Meggers, E. Direct Visible-Light-Excited Asymmetric Lewis Acid Catalysis of Intermolecular [2+2] Photocycloadditions. *J. Am. Chem. Soc.* **2017**, *139*, 9120–9123; (c) Zheng, J.; Swords, W. B.; Jung, H.; Skubi, K. L.; Kidd, J. B.; Meyer, G. J.; Baik, M.-H.; Yoon, T. P. Enantioselective Intermolecular Excited-State Photoreactions Using a Chiral Ir Triplet Sensitizer: Separating Association from Energy Transfer in Asymmetric Photocatalysis. *J. Am. Chem. Soc.* **2019**, *141*, 13625–13634.
11. (a) Molloy, J. J.; Morack, T.; Gilmour, R. Positional and Geometrical Isomerisation of Alkenes: The Pinnacle of Atom Economy. *Angew. Chem. Int. Ed.* **2019**, *58*, 13654–13664; (b) Neveselý, T.; Wienhold, M.; Molloy, J. J.; Gilmour, R. Advances in the E → Z Isomerization of Alkenes Using Small Molecule Photocatalysts. *Chem. Rev.* **2021**, *122*, 2650–2694; (c) Livingstone, K.; Tenberge, M.; Pape, F.; Daniliuc, C. G.; Jamieson, C.; Gilmour, R. Photocatalytic E → Z Isomerization of β-Ionyl Derivatives. *Org. Lett.* **2019**, *21*, 9677–9680; (d) Kweon, B.; Blank, L.; Soika, J.; Messara, A.; Daniliuc, C. G.; Gilmour, R. Regio- and Stereo-Selective Isomerization of Borylated 1,3-Dienes Enabled by Selective Energy TransferCatalysis. *Angew. Chem. Int. Ed.* **2024**, *63*, e202404233.
12. (a) Sicignano, M.; Rodríguez, R. I.; Alemán, J. Recent Visible Light and Metal Free Strategies in [2+2] and [4+2] Photocycloadditions. *Eur. J. Org. Chem.* **2021**, *2021*, 3303–3321; (b) Lin, S.; Ischay, M. A.; Fry, C. G.; Yoon, T. P. Radical Cation Diels–Alder Cycloadditions by Visible Light Photocatalysis. *J. Am. Chem. Soc.* **2011**, *133*, 19350–19353; (c) Zhao, Y.; Antonietti, M. Visible-Light-Irradiated Graphitic Carbon Nitride Photocatalyzed Diels–Alder Reactions with Dioxygen as Sustainable Mediator for Photoinduced Electrons. *Angew. Chem. Int. Ed.* **2017**, *56*, 9336–9340; (d) Jiang, Y.; Yang, M.; Wu, Y.; López-Arteaga, R.; Rogers, C. R.; Weiss, E. A. Chemo- and Stereoselective Intermolecular [2 + 2] Photocycloaddition of Conjugated Dienes Using Colloidal Nanocrystal Photocatalysts. *Chem Catal.* **2021**, *1*, 106–116.
13. For a recent review on energy transfer in organic synthesis see: Dutta, S.; Erchinger, J. E.; Strieth-Kalthoff, F.; Kleinmans, R.; Glorius, F. Energy Transfer Photocatalysis: Exciting Modes of Reactivity. *Chem. Soc. Rev.* **2024**, *53*, 1068–1089.
14. (a) Ma, J.; Chen, S.; Bellotti, P.; Guo, R.; Schäfer, F.; Heusler, A.; Zhang, X.; Daniliuc, C.; Brown, K. M.; Houk, N. K.; Glorius, F. Photochemical Intermolecular Dearomative Cycloaddition of Bicyclic Azaarenes with Alkenes. *Science* **2021**, *371*, 1338–1345; (b) Guo, R.; Adak, S.; Bellotti, P.; Gao, X.; Smith, W. W.; Le, S. N.; Ma, J.; Houk, K. N.; Glorius, F.; Chen, S.; Brown, M. K.

Photochemical Dearomative Cycloadditions of Quinolines and Alkenes: Scope and Mechanism Studies. *J. Am. Chem. Soc.* **2022**, *144*, 17680–17691; (c) Wang, W.; Cai, Y.; Guo, R.; Brown, M. K. Synthesis of Complex Bicyclic Scaffolds by Intermolecular Photosensitized Dearomative Cycloadditions of Activated Alkenes and Naphthalenes. *Chem. Sci.* **2022**, *13*, 13582–13587; (d) Wang, W.; Brown, M. K. Photosensitized [4+2]- and [2+2]-Cycloaddition Reactions of N-Sulfonylimines. *Angew. Chem. Int. Ed.* **2023**, *62*, e202305622. (e) Schlosser, L.; Rana, D.; Pflüger, P.; Katzenburg, F.; Glorius, F. EnTdecker − A Machine Learning-Based Platform for Guiding Substrate Discovery in Energy Transfer Catalysis. *J. Am. Chem. Soc.* **2024**, *146*, 13266–13275.

15. (a) Molloy, J. J.; Metternich, J. B.; Daniliuc, C. G.; Watson, A. J. B.; Gilmour, R. Contra-Thermodynamic, Photocatalytic E→Z Isomerization of Styrenyl Boron Species: Vectors to Facilitate Exploration of Two-Dimensional Chemical Space. *Angew. Chem. Int. Ed.* **2018**, *57*, 3168–3172; (b) Molloy, J. J.; Schäfer, M.; Wienhold, M.; Morack, T.; Daniliuc, C. G.; Gilmour, R. Boron-Enabled Geometric Isomerization of Alkenes via Selective Energy-Transfer Catalysis. *Science* **2020**, *369*, 302–306; (c) Zähringer, T. J. B.; Wienhold, M.; Gilmour, R.; Kerzig, C. Direct Observation of Triplet States in the Isomerization of Alkenylboronates by Energy Transfer Catalysis. *J. Am. Chem. Soc.* **2023**, *145*, 21576–21586; (d) Liu, Y.; Ni, D.; Stevenson, B. G.; Tripathy, V.; Braley, S. E.; Raghavachari, K.; Swierk, J. R.; Brown, M. K. Photosensitized [2+2]-Cycloadditions of Alkenylboronates and Alkenes. *Angew. Chem. Int. Ed.* **2022**, *61*, e202200725; (e) Posz, J. M.; Sharma, N.; Royalty, P. A.; Liu, Y.; Salome, C.; Fessard, T. C.; Brown, M. K. Synthesis of Borylated Carbocycles by [2 + 2]-Cycloadditions and Photo-Ene Reactions. *J. Am. Chem. Soc.* **2024**, *146*, 10142–10149; (f) Hanania, N.; Eghbarieh, N.; Masarwa, A. PolyBorylated Alkenes as Energy-Transfer Reactive Groups: Access to Multi-Borylated Cyclobutanes Combined with Hydrogen Atom Transfer Event. *Angew. Chem. Int. Ed.* **2024**, *63*, e202405898.
16. (a) Kumar, N.; Reddy, R. R.; Eghbarieh, N.; Masarwa, A. α-Borylalkyl Radicals: Their Distinctive Reactivity in Modern Organic Synthesis. *Chem. Commun.* **2020**, *56*, 13–25; (b) Lovinger, G. J.; Morken, J. P. Recent Advances in Radical Addition to Alkenylboron Compounds. *Eur. J. Org. Chem.* **2020**, *2020*, 2362–2368; (c) Quiclet-Sire, B.; Zard, S. Z. Radical Instability in Aid of Efficiency: A Powerful Route to Highly Functional MIDA Boronates. *J. Am. Chem. Soc.* **2015**, *137*, 6762–6765; (d) Kischkewitz, M.; Okamoto, K.; Mück-Lichtenfeld, C.; Studer, A. Radical-Polar Crossover Reactions of Vinylboron Ate Complexes. *Science* **2017**, *355*, 936–938; (e) Silvi, M.; Sandford, C.; Aggarwal, V. K. Merging Photoredox with 1,2-Metallate Rearrangements: The Photochemical Alkylation of Vinyl Boronate Complexes. *J. Am. Chem. Soc.* **2017**, *139*, 5736–5739; (f) Gerleve, C.; Kischkewitz, M.; Studer, A. Synthesis of α-Chiral Ketones and Chiral Alkanes Using Radical Polar Crossover Reactions of Vinyl Boron Ate Complexes. *Angew. Chem. Int. Ed.* **2018**, *57*, 2441–2444; (g) Noble, A.; Mega, R. S.; Pflästerer, D.; Myers, E. L.; Aggarwal, V. K. Visible-Light-Mediated Decarboxylative Radical Additions to Vinyl Boronic Esters: Rapid Access to γ-Amino Boronic Esters. *Angew. Chem. Int. Ed.* **2018**, *57*, 2155–2159; (h) Marotta, A.; Fang, H.; Adams, C. E.; Sun Marcus, K.; Daniliuc, C. G.; Molloy, J. J. Direct Light-Enabled Access to α-Boryl Radicals: Application in the Stereodivergent Synthesis of Allyl Boronic Esters. *Angew. Chem. Int. Ed.* **2023**, *62*, e202307540; (i) McGhie, L.; Marotta, A.; Loftus, P. O.; Seeberger, P. H.; Funes-Ardoiz, I.; Molloy, J. J. Photogeneration of α-Bimetalloid Radicals via Selective Activation of Multifunctional C1 Units. *J. Am. Chem. Soc.* **2024**, *146*, 15850–15859.
17. Teegardin, K.; Day, J. I.; Chan, J.; Weaver, J. Advances in Photocatalysis: A Microreview of Visible Light Mediated Ruthenium and Iridium Catalyzed Organic Transformations. *Org. Process Res. Dev.* **2016**, *20*, 1156–1163.
18. Hörmann, F. M.; Kerzig, C.; Chung, T. S.; Bauer, A.; Wenger, O. S.; Bach, T. Triplet Energy Transfer from Ruthenium Complexes to Chiral Eniminium Ions: Enantioselective Synthesis of Cyclobutanecarbaldehydes by [2+2] Photocycloaddition. *Angew. Chem. Int. Ed.* **2020**, *59*, 9659–9668.
19. (a) Zan, L.; Chao, Z.; Tao, L.; Xiao-Lei, N.; Bin, C.; Chen-Ho, T.; Li-Zhu, W. Aggregation-Enabled Intermolecular Photo[2+2]Cycloaddition of Aryl Terminal Olefins by Visible-Light Catalysis. *CCS Chem.* **2019**, *2*, 582–588; (b) Mandigma, M. J. P.; Kaur, J.; Barham, J. P. Organophotocatalytic Mechanisms: Simplicity or Naïvety? Diverting Reactive Pathways by Modifications of Catalyst Structure, Redox States and Substrate Preassemblies. *ChemCatChem* **2023**, *15*, e202201542; (c) Wylie, L.; Barham, J. P.; Kirchner, B. Solvent Dependency of Catalyst-Substrate Aggregation Through π-π Stacking in Photoredox Catalysis. *ChemPhysChem* **2023**, *24*, e202300470; (d) Yakubov, S.; Dauth, B.; Stockerl, W. J.; da Silva, W.; Gschwind, R. M.; Barham, J. P. Protodefluorinated Selectfluor® Aggregatively Activates Selectfluor® for Efficient Radical C(Sp3)−H Fluorination Reactions. *ChemSusChem* **2024**, e202401057.
20. X-ray analysis revealed that crystal packing also favored head to tail due to the steric constraints of the *geminal* boronic ester (See ESI for full details, Figure S10b).
21. (a) Kleinmans, R.; Pinkert, T.; Dutta, S.; Paulisch, T. O.; Keum, H.; Daniliuc, C. G.; Glorius, F. Intermolecular [2π+2σ]-Photocycloaddition Enabled by Triplet Energy Transfer. *Nature* **2022**, *605*, 477–482; (b) Guo, R.; Chang, Y.-C.; Herter, L.; Salome, C.; Braley, S. E.; Fessard, T. C.; Brown, M. K. Strain-Release [2π + 2σ] Cycloadditions for the Synthesis of Bicyclo[2.1.1]Hexanes Initiated by Energy Transfer. *J. Am. Chem. Soc.* **2022**, *144*, 7988–7994; (c) Golfmann, M.; Walker, J. C. L. Bicyclobutanes as Unusual Building Blocks for Complexity Generation in Organic Synthesis. *Commun. Chem.* **2023**, *6*, 9; (d) Bellotti, P.; Glorius, F. Strain-Release Photocatalysis. *J. Am. Chem. Soc.* **2023**, *145*, 20716–20732; (e) de Robichon, M.; Kratz,

T.; Beyer, F.; Zuber, J.; Merten, C.; Bach, T. Enantioselective, Intermolecular [Π2+σ2] Photocycloaddition Reactions of 2(1H)-Quinolones and Bicyclo[1.1.0]Butanes. *J. Am. Chem. Soc.* **2023**, *145*, 24466–24470.

22. For the use of BMIDA reagents in synthesis see: (a) Gillis, E. P.; Burke, M. D. A Simple and Modular Strategy for Small Molecule Synthesis: Iterative Suzuki−Miyaura Coupling of B-Protected Haloboronic Acid Building Blocks. *J. Am. Chem. Soc.* **2007**, *129*, 6716–6717; (b) Li, J.; Ballmer, S. G.; Gillis, E. P.; Fujii, S.; Schmidt, M. J.; Palazzolo, A. M. E.; Lehmann, J. W.; Morehouse, G. F.; Burke, M. D. Synthesis of Many Different Types of Organic Small Molecules Using One Automated Process. *Science* **2015**, *347*, 1221–1226; (c) Lee, C. F.; Diaz, D. B.; Holownia, A.; Kaldas, S. J.; Liew, S. K.; Garrett, G. E.; Dudding, T.; Yudin, A. K. Amine Hemilability Enables Boron to Mechanistically Resemble Either Hydride or Proton. *Nat. Chem.* **2018**, *10*, 1062–1070; (d) Blair, D. J.; Chitti, S.; Trobe, M.; Kostyra, D. M.; Haley, H. M. S.; Hansen, R. L.; Ballmer, S. G.; Woods, T. J.; Wang, W.; Mubayi, V.; Schmidt, M. J.; Pipal, R. W.; Morehouse, G. F.; Palazzolo Ray, A. M. E.; Gray, D. L.; Gill, A. L.; Burke, M. D. Automated Iterative Csp3–C Bond Formation. *Nature* **2022**, *604*, 92–97; (e) Trofimova, A.; White, B.; Diaz, D. B.; Širvinskas, M. J.; Lough, A.; Dudding, T.; Yudin, A. K. A Boron Scan of Ethyl Acetoacetate Leads to Versatile Building Blocks. *Angew. Chem. Int. Ed.* **2024**, *63*, e202319842.
23. (a) Metternich, J. B.; Gilmour, R. A Bio-Inspired, Catalytic E → Z Isomerization of Activated Olefins. *J. Am. Chem. Soc.* **2015**, *137*, 11254–11257; (b) Metternich, J. B.; Artiukhin, D. G.; Holland, M. C.; von Bremen-Kühne, M.; Neugebauer, J.; Gilmour, R. Photocatalytic E → Z Isomerization of Polarized Alkenes Inspired by the Visual Cycle: Mechanistic Dichotomy and Origin of Selectivity. *J. Org. Chem.* **2017**, *82*, 9955–9977.
24. (a) Richardson, A. D.; Becker, M. R.; Schindler, C. S. Synthesis of Azetidines by Aza Paternò–Büchi Reactions. *Chem. Sci.* **2020**, *11*, 7553–7561; (b) Becker, M. R.; Richardson, A. D.; Schindler, C. S. Functionalized Azetidines via Visible Light-Enabled Aza Paternò-Büchi Reactions. *Nat. Commun.* **2019**, *10*, 5095; (c) Becker, M. R.; Wearing, E. R.; Schindler, C. S. Synthesis of Azetidines via Visible-Light-Mediated Intermolecular [2+2] Photocycloadditions. *Nat. Chem.* **2020**, *12*, 898–905; (d) Wearing, E. R.; Yeh, Y.-C.; Terrones, G. G.; Parikh, S. G.; Kevlishvili, I.; Kulik, H. J.; Schindler, C. S. Visible Light–Mediated Aza Paternò–Büchi Reaction of Acyclic Oximes and Alkenes to Azetidines. *Science* **2024**, *384*, 1468–1476.
25. For recent theoretical investigations of energy transfer see: (a) Popescu, M. V; Paton, R. S. Dynamic Vertical Triplet Energies: Understanding and Predicting Triplet Energy Transfer. *Chem* **2024**; (b) Meyer, A. R.; Popescu, M. V; Sau, A.; Damrauer, N. H.; Paton, R. S.; Yoon, T. P. Combined Synthetic, Spectroscopic, and Computational Insights Into a General Method for Photosensitized Alkene Aziridination. *ACS Catal.* **2024**, 12310–12317.
26. Rodríguez-Guerra, J. Jaimergp/Easymecp: V0.3.2. Zenodo November **2020.**
27. (a) Sun, C.; Potter, B.; Morken, J. P. A Catalytic Enantiotopic-Group-Selective Suzuki Reaction for the Construction of Chiral Organoboronates. *J. Am. Chem. Soc.* **2014**, *136*, 6534–6537; (b) Nallagonda, R.; Padala, K.; Masarwa, A. Gem-Diborylalkanes: Recent Advances in Their Preparation, Transformation and Application. *Org. Biomol. Chem.* **2018**, *16*, 1050–1064; (c) Zhang, C.; Hu, W.; Morken, J. P. α-Boryl Organometallic Reagents in Catalytic Asymmetric Synthesis. *ACS Catal.* **2021**, *11*, 10660–10680; (d) Hong, K.; Liu, X.; Morken, J. P. Simple Access to Elusive α-Boryl Carbanions and Their Alkylation: An Umpolung Construction for Organic Synthesis. *J. Am. Chem. Soc.* **2014**, *136*, 10581–10584.
28. For recent mechanistic studies on protodeboronation see: (a) Cox, P. A.; Leach, A. G.; Campbell, A. D.; Lloyd-Jones, G. C. Protodeboronation of Heteroaromatic, Vinyl, and Cyclopropyl Boronic Acids: PH–Rate Profiles, Autocatalysis, and Disproportionation. *J. Am. Chem. Soc.* **2016**, *138*, 9145–9157; (b) Cox, P. A.; Reid, M.; Leach, A. G.; Campbell, A. D.; King, E. J.; Lloyd-Jones, G. C. Base-Catalyzed Aryl-B(OH)2 Protodeboronation Revisited: From Concerted Proton Transfer to Liberation of a Transient Aryl Anion. *J. Am. Chem. Soc.* **2017**, *139*, 13156–13165; (c) Hayes, H. L. D.; Wei, R.; Assante, M.; Geogheghan, K. J.; Jin, N.; Tomasi, S.; Noonan, G.; Leach, A. G.; Lloyd-Jones, G. C. Protodeboronation of (Hetero)Arylboronic Esters: Direct versus Prehydrolytic Pathways and Self-/Auto-Catalysis. *J. Am. Chem. Soc.* **2021**, *143*, 14814–14826.